Copper oxide nanomaterial fate in plant tissue: nanoscale impacts on reproductive tissues

Copper Oxide nanomaterial fate in plant tissue: Nanoscale impacts on reproductive tissues

Marta Marmiroli,[1,*] Luca Pagano,[1,*] Riccardo Rossi,[1] Roberto De La Torre-Roche,[2] Giovanni Orazio Lepore,[3] Roberta Ruotolo,[1] Gianluca Gariani,[4] Valentina Bonanni,[4] Simone Pollastri,[4] Alessandro Puri,[5] Alessandra Gianoncelli,[4] Giuliana Aquilanti,[4] Francesco d'Acapito,[5] Jason C. White,[2,§] Nelson Marmiroli[1,6,§,#]

[1] Department of Chemistry, Life Sciences and Environmental Sustainability, University of Parma, Parco Area delle Scienze 11/A, 43124 Parma, Italy.

[2] The Connecticut Agricultural Experiment Station, 123 Huntington Street, 06504 New Haven, CT, USA.

[3] Earth Science Department, Univeristy of Florence, Via La Pira 4, 50121 Firenze, Italy.

[4] Elettra, Sincrotrone Trieste, Strada Statale 14 - km 163,5 in AREA Science Park, 34149 Trieste, Italy.

[5] CNR-IOM-OGG c/o ESRF – The European Synchrotron, 71 Avenue des Martyrs CS 40220, F-38043 Grenoble Cédex 9, France.

[6] Consorzio Interuniversitario Nazionale per le Scienze Ambientali (CINSA), University of Parma, 43124 Parma, Italy.

* co-first authorship.

§ co-last authorship.

corresponding author, nelson.marmiroli@unipr.it.

Abstract

A thorough understanding of the implications of chronic low dose exposure to Engineered Nanomaterials (ENMs) through the food chain is lacking. The present study aimed to characterize such response in *Cucurbita pepo* L. (zucchini) upon exposure to a commonly researched nanoscale fertilizer: copper oxide (CuO) nanoparticles. Zucchini was grown in soil amended with nano-CuO, bulk CuO and $CuSO_4$ from seed germination to flowering stage. Nano-CuO treatment had no impact on plant morphology or growth, nor pollen formation and viability. The uptake of Cu was comparable in the plant tissues, under all treatments. RNA-seq analyses on vegetative and reproductive tissues

highlighted a nanoscale-specific component of the response, where mitochondrial and chloroplast functions were uniquely modulated in response to nanomaterial exposure as compared with conventional bulk and salt forms of the nutrient. EXAFS spectroscopy showed that Cu local structure changed upon CuO nanoparticles (NPs) internalization. These findings demonstrate the physiological, cellular, and molecular consequences related to nano-CuO application as a plant fertilizer and highlight the need to understand the mechanism of plant response to minimize environmental and health risk and to ensure development sustainable nano-enabled agricultural strategies.

Keywords: nanomaterials, nanofertilization, RNA-seq, pollen, biotransformation, *Cucurbita pepo.*

Synopsis

Fertilization with nanoscale CuO affected zucchini at the physiological and molecular levels, from roots to flowers, with significant internalization and particle biotransformation being evident.

Introduction

In the recent years, interest in the utilization of nanotechnology to produce nano-enabled materials and delivery platforms to address the progressive inefficiency of mineral fertilization has been rapidly growing.[1,2] However, these nanomaterials are by their very nature more reactive than traditional ones, bioavailable, and as such, have raised concerns over sustainability and safety with regard to human and environmental health. For example, direct utilization in agriculture raises the clear possibility of food chain contamination from staple plants to humans through the direct consumption of contaminated plant products as could happen with rice, maize and peanuts.[3,4] In addition, the potential widespread use of engineered nanomaterials (ENMs) as part of "nano-agricultural chemistry" has created concerns over damage to non-target organisms and to potential trophic transfer through terrestrial food chains, through vegetables grazing by simple insects and then spreading out to higher insects and predators.[5-9] As such, safety assessment and sustainability evaluation must be a core component in novel materials formulations for agri-food production purposes (e.g. nanopesticides, nanofertilizers). [1,10-13]

A number of recent studies have demonstrated the unique potential of Cu-based nanomaterials in agriculture,[11,14,15] including field studies demonstrating how materials such as $Cu_3(PO4)_2$ based-nanosheets and commercial CuO NPs can be foliar applied to young seedlings so as to increase plant growth and suppress *Fusarium* spp. infections of tomato (*Solanum lycopersicum* L.) and watermelon (*Citrullus lanatus* L.) in full life cycle studies. Furthermore, Ma *et al*. (2020)[13] studied how nanomaterial chemistry could be tuned to optimize the effects of pathogen suppression and nutrient release from Cu-based ENMs on sudden death disease (SDS) in soybean (*Glycine max* L.), developing a thermodynamic model to describe how morphology and matrix effects are implicated in Cu release and plant response. In addition, Cu-based nanoformulations are known to interact with organic acids in plant root exudates. These interactions significantly influence ENM stability,

biotransformation and bioavailability,[16] as well as induce modifications in the plant metabolome.[17] The role of Cu nanomaterial bioavailability has also been investigated through trophic transfer experiments, including an assessment of how initial chemical form is impacted by relevant weathering conditions and subsequent material transformation.[18] These findings highlight the importance of controlling ENMs physico-chemical properties (e.g. morphology, composition and dissolution) so as to develop safer and more sustainable nanoscale formulations for agriculture, simultaneously enhancing the targeting and delivery efficiency to optimize utilization of resources while minimizing negative impacts on the environment.[1]

The current study investigated the potential effects of CuO NPs on zucchini (*Cucurbita pepo* L.) from a morphological, physiological, molecular, and atomic perspective, with a particular focus on gametogenesis and pollen development. Conventional CuO bulk material and $CuSO_4$ salts were used as controls to clarify nanoscale-specific effects of CuO NPs with regard to its fate within the plant tissues. Particular attention was focused on the function and regulation of chloroplast and mitochondrion activity, which play a critical role in pollen development. The coupling of a transcriptomic approach (by RNA-seq) with synchrotron-based analyses such as μ-X-ray Fluorescence (μ-XRF) mapping and Extended X-ray absorption fine structure (EXAFS) spectroscopy, of Cu state in different tissues maximized resolution at the molecular and sub-molecular levels and enabled a thorough understanding of the connection between the observed biological response and the physico-chemical condition of CuO NPs in the different plant tissues.

Methods

Nanomaterial characterization

Copper oxide nanoparticles (CuO NPs) (99% purity; 40 nm average sized) were purchased from U.S. Research Nanomaterials, Inc. (Houston, TX). Cu represent 79.8% of the total molecular weight of the molecule. CuO NPs were characterized by electron microscopy (TEM, Talos F200S G2, SEM FEG Thermo Fisher Scientific, Waltham, MA, USA) as reported in Figure S1. The average

particle size (*dh*) and zeta (ζ) potential were 533.9 nm and of -24.7 mV in ddH_2O as determined on a Zetasizer Nano Series ZS90 (Malvern Instruments, Malvern, UK). CuO bulk material and $CuSO_4 \cdot 5H_2O$ were purchased from Sigma Aldrich (St. Louis, MO, US).

For particle dissolution analysis, CuO NPs and CuO bulk solutions (1000 mg L^{-1}) were prepared in ddH_2O, avoiding shaking and light, and portions were collected after 1, 2, 3, 7, and 14d. Aliquots of 1 ml for each sample were precipitated by ultracentrifugation at 30000 rpm, for 10 min, at 20°C (Optima Max-XP Ultracentrifuge, Beckman-Coulter Inc., Brea, CA, USA). The liquid phase was collected and digested in 4 mL of 1M HNO_3 for 40 min at 200°C using a VELP DK20 digester (VELP Scientifica, Usmate, Italy). The digests were analysed by flame atomic absorption spectroscopy (FA-AAS; AA240FS, Agilent Technologies, Santa Clara, CA, USA) for the presence of Cu (linearity of calibration, R^2: 0.9982). The average dissolution for CuO bulk and CuO NPs were between 0.1% and 0.15%, respectively, considering the theoretical value of 100% dissolution of ionic copper in $CuSO_4$.

Plant exposure

Cucurbita pepo L. (cv. Costata Romanesco) seeds were pre-germinated in vermiculite for 10 days prior to transplanting to soil. Zucchini seeds were purchased from Johnny's Selected Seeds (Albion, ME, USA). The experimental soil was collected from the Connecticut Agricultural Experiment Station (CAES) Lockwood Farm in Hamden, CT, USA. Individual solutions of CuO NPs and CuO bulk material in water (30% water capacity of soil/vermiculite mixture) were probe sonicated by a Fisher Scientific Model 505 Sonic Dismembrator (Fisher Scientific, Waltham, MA) at 40% amplitude for 60−120s to maximize dispersion. Solutions of CuO NPs, CuO (bulk) or (copper sulfate) $CuSO_4$ were slowly added to pots containing 500g of soil. The final concentration of NPs and bulk CuO in pots was 100 mg kg^{-1} while for $CuSO_4 \cdot 5H_2O$ (copper sulfate pentahydrate), the amount was 320 mg kg^{-1}. Considering the molecular weight of the single molecules taken into account, this

represented a total concentration of approximately 80 mg kg^{-1} for all the treatments. The concentrations utilized were chosen to be below the limit considered as potential Cu contamination in soil.[19-20] Furthermore, the low dose utilized and the long growth period (60 days) are indicative of a chronic exposure scenario that is not common in the literature.[21] Zucchini seedlings were planted (one each pot) and grown indoor under supplemental fluorescent lighting (60 μE m^2 sec) under a photoperiod of 16h light at approximately 22−28 °C until flowering. The plants were top watered and amended every two weeks with Hoagland's Solution (10%) during a 60-d growth period. For every condition, 10 biological replicates were included.

Pollen morphology and pollen viability

Alexander's staining protocol was used to test pollen viability. Free anthers were collected when pollen was mature but anthers were still non-dehiscent (stage 12-13), and were fixed in Carnoy's fixative (6 ethanol: 3 chloroform: 1 acetic acid) for 2h. Mature pollen was collected and stained as described in Peterson *et al* (2010).[22] After staining, all aborted and non-aborted pollen grains were counted using a Zeiss Apotome 2 microscope at 20x magnification (Zeiss, Oberkochen, Germany). Pollen grains were analysed fresh with no fixation or staining; they were collected from mature flowers and positioned on 2 cm diameter stainless-steel sample holder (stub) covered with adhesive carbon tape. An environmental scanning electron microscope (ESEM) FEG2500 FEI (FEI Europe, Eindhoven, The Netherlands) operating in low-vacuum (60 Pa) with LFD (Large Field Detector) was used to enable optimal Secondary Electron (SE) imaging. The cone PLA (Pressure Limiting Aperture) of 500 μm improved the signal available to the Bruker X-ray detector, QUANTAX XFlash. SE imaging was performed at 10 KeV with a beam size of 2.5 μm, EDX analysis at 20 KeV acceleration voltage, final lens aperture of 40 μm, and beam size of 4 μm. SE images and EDX spectra were collected from samples treated with CuO NPs, CuO bulk and untreated controls.

Metal uptake measurement

Flowers harvested for elemental analyses were sampled and thoroughly rinsed with tap water, MilliQ water and 2% HNO_3 (0.01 M) to remove soil and surface-attached NPs. To determine Cu content in the tissues, fresh samples were dried at 100 °C for 72 h and digested in HNO_3 at 115 °C, 25 min. After 30 min, 1 mL of 20% H_2O_2 was added to each digestion tube and the samples treated for an additional 30 min prior dilution to 50 mL with ddH_2O. The digested samples from the 10 biological replicates per treatment were analysed by inductively coupled plasma mass spectrometry (ICP-MS) Agilent 7500ce (Agilent Technologies, Santa Clara, CA) for Cu presence (63 amu). Roots, stems, leaves and flower biomass samples were collected after 60-d for elemental analysis. Samples were digested as previously reported and analysed by Atomic Adsorption Spectroscopy (AAS) (AA240FS device, Agilent Technologies, Santa Clara, CA) with a wavelength of 324.8 nm. All analyses were conducted with a four-point calibration curve based on standard reference material (SPEX CertiPrep, Metuchen, NJ). Biomass and Cu content in all tissues were evaluated by a one-way ANOVA with a pairwise Tukey's multiple comparison test (IBM SPSS v. 26.0).

RNA extraction and whole transcriptome analysis

RNA samples were extracted from 0.1g (fresh weight) of pollen, leaves or roots samples from unamended control, CuO NP, CuO bulk and $CuSO_4$ treatments. Total RNA was extracted from 0.1 g of fresh plant material using a Sigma-Aldrich Spectrum Plant Total RNA Kit (Sigma-Aldrich, St. Louis, MO). Three biological replicates per treatment were used. Total RNA quality was assessed by gel electrophoresis and RNA quantity was determined using a Thermo Scientific Nanodrop Lite Spectrophotometer (Thermo Fisher Scientific, Wilmington, DE). Samples were sent to IGA Technologies Srl (Udine, IT) for RNA sequencing service. TruSeq Stranded mRNA kit (Illumina, San Diego, CA) was used for library preparation following the manufacturer's instructions. RNA samples were quantified and quality tested by Agilent 2100 Bioanalyzer RNA assay (Agilent

Technologies, Santa Clara, CA). Final libraries were checked Agilent Bioanalyzer DNA assay (Agilent Technologies, Santa Clara, CA). Libraries were prepared for sequencing and sequenced on single-end 75 bp mode on NextSeq 500 (Illumina, San Diego, CA). Alignment of reads to the reference transcriptome available on Cucurbitgenomics database (http://cucurbitgenomics.org/)[23] was performed using STAR software with default parameters. The resulting raw data have been normalized and the differentially expressed genes were identified using a 2.3 threshold of FPKM data (in log2). Data have been deposited in the NCBI GEO database (accession number …).

A student *t* test was applied for analysis of homogeneity of variance, statistical analysis for scatter plots, box and whiskers graphs. A principal component analysis (PCA) was performed with R statistical software (www.r-project.org). Venny bioinformatics tool (http://bioinfogp.cnb.csic.es/tools/venny/) was used for the generation of Venn diagrams. Gene Ontology (GO) analysis and *A. thaliana* ortholog gene identification was performed by the Cucurbitgenomics database. The GO term enrichment analysis was conducted using a cut-off p-value of 0.05 for cellular components and biological processes, and 0.03 for relevant pathways, respectively. Network analysis was performed using the GeneMANIA data service (http://www.genemania.org/) using *A. thaliana* orthologues genes.

Samples preparation for synchrotron-based analyses

Roots, leaf and flower samples (0.1 g, fresh weight) were cut and submerged in glutaraldehyde triphosphate into Eppendorf tubes for fixation. After three days the samples were dehydrated in gradients of alcohol (from 25 to 100%) and fixed with epoxy resin following Kurth et al. (2009).[24] For X-ray Absorption Spectroscopy (XAS) analyses at BM08 "LISA" beamline at ESRF, the protocols described in Marmiroli et al. (2020)[25] were applied. Briefly, samples were mixed with pure cellulose powder (Sigma Aldrich, St. Louis, MO, USA) and pressed into 1.3 cm diameter pellets using an amount of material sufficient to keep the total absorption (μ) $\leq$1.5 above the edge.

206

207 *Low Energy μ-XRF (LE μ-XRF)*

208 XRF analyses were performed at the TwinMic beamline at ELETTRA, Sincrotrone Trieste,
209 Italy.[26] For the present experiment, the TwinMic microscope was operated in scanning transmission
210 mode (SXM), the beam was focused on the sample through a zone plate (600 μm in diameter with a
211 50 nm outermost zone width), and a micrometric or sub-micrometric probe size was delivered. While
212 the sample was raster-scanned perpendicularly to the incoming monochromatic beam, a fast readout
213 CCD camera collected the transmitted X-rays and an 8-silicon drift detector-based XRF system
214 acquired the emitted fluorescence photons.[27] The obtained absorption and phase contrast images
215 outline the morphological features of the sample at sub-micrometer length scales, whereas the
216 simultaneous detection of the low energy XRF correlates the elemental distribution to the
217 morphology. The elemental distribution was then obtained by deconvolving and fitting the XRF
218 spectra with PyMCA software.[28] A photon energy of 1.26 keV was used to excite and obtain optimal
219 emission conditions for the elements of major interest (Cu, Na, Ni and Fe) with a spot size of 1.45
220 μm and a dwell time of 8 s per pixel for XRF mapping and a CCD dwell time of 50 ms per SXM
221 imaging. Each map lasted approximately 5-7 h, depending on the dimensions of the scanned area.

222

223 *XRF and X-ray absorption near edge structure (XANES) mapping*

224 Zucchini root and flower thin section samples were investigated by means of XRF mapping
225 and XAS. The experiment was conducted using a Si(111) monochromator and standard 45º/45º
226 geometry for fluorescence mode measurements, using an XFlash 5030 SDD (Bruker, Berlin,
227 Germany). Thin sections of samples embedded in resin were sealed between two Mylar foils and
228 fixed on the Al sample holder using a Delrin interlocking ring. This design was necessary to secure
229 the samples and to have a system compatible with the working conditions of the Ultra High Vacuum

Chamber (UHVC, 10^{-7} mbar) available at the XRF beamline, ELETTRA Sincrotrone Trieste (Italy).[29] XRF maps were collected with an incident beam energy of 10 keV and a beam size at the exit slits of 200x100 μm^2 (HxV); on one selected sample an additional map with higher spatial resolution of 100x50 μm^2 was also collected. Higher order harmonics contamination was suppressed by a pair of parallel plane mirrors intercepting the beam in grazing incidence. Orienting on the basis of the element distribution in the samples, the areas with higher content of Fe, Cu and Zn were selected to collect XANES spectra at the relative K-edges. The Si(111) monochromator was calibrated before the measurements using reference metal foils. All spectra were collected using 5 seconds per step and a variable energy step as a function of the energy: Large step (5 eV) in the first 200 eV of the spectrum, smaller step (0.2 eV) in the near-edge region and a k-constant step of 0.07 $Å^{-1}$ further above the absorption edge. Multiple spectra were collected and merged in order to increase the signal to noise ratio. The oxidation state was determined using least-squares Linear Combination Fitting (LCF) based on reference spectra collected on compounds of known oxidation state. Background removal, normalization of XANES spectra and LCF analyses were performed using the ATHENA software package.[30]

XAS and extended X-ray absorption fine structure (EXAFS)

X-ray Absorption Spectroscopy (XAS) measurements at the Cu K-edge (8978.9 eV) were performed at the LISA CRG beamline (BM08)[31] at the European Synchrotron Radiation Facility (ESRF, Grenoble, France) using plant samples and three model compounds: CuO (bulk), CuO NPs and $CuSO_4 \cdot 5H_2O$. The main optical features of the beamline were a fixed exit monochromator with a pair of Si(111) crystals (energy resolution $\Delta E/E \approx 1.33 \cdot 10^{-4}$); Si mirrors were used for harmonics rejection (E cutoff ≈ 15 KeV). Energy was calibrated with a Cu reference foil (8978.9 eV). Spectra of plant samples were acquired at 80 K, in order to minimize beam-induced damage, with a constant k step of 0.05 $Å^{-1}$ up to a maximum k value of 12.5 $Å^{-1}$; model compounds were measured at room

temperature with a k step of 0.03 $Å^{-1}$ up to k=18 $Å^{-1}$. Plant samples were measured in fluorescence mode with a 12-element HP-Ge detector,[32] while model compounds were measured in transmission mode. Multiple spectra were collected and merged in order to increase the signal to noise ratio. ATHENA software[33] was used to calibrate the energy and to average multiple spectra. Standard procedures were followed to extract the structural extended EXAFS signals ($k \cdot \chi(k)$), including pre-edge background removal, spline modelling of bare atomic background, edge step normalization, and energy calibration.[33] Model atomic clusters centered on the absorber atom were obtained by ATOMS;[34] theoretical amplitude and phase functions were generated using the FEFF8 code.[36] EXAFS spectra were fitted through the ARTEMIS software in the Fourier-Transform (FT) space.[30]

Results and Discussion

Pollen morphology and viability

Pollen grain morphology was analysed by ESEM of transverse sections of developing mature anthers; no overt differences were observed across treatments (Figure S2a). Pollen viability was also evaluated to determine the male gametophyte developmental stage and the preservation of plant reproductive fitness. Similar to morphology, there were no differences across CuO NP, CuO bulk and $CuSO_4$ treatments as compared to the untreated control, with a pollen viability approximately 100% in all cases (Figure S2b).

Previous studies have demonstrated that copper can be toxic to seed and pollen germination, pollen viability and pollen tube growth; Sharafi (2014)[36] showed that high concentrations (250 mg kg^{-1}) of copper cause an almost complete inhibition of pollen germination and pollen tube lengthening in almond (*Prunus dulcis* (Mill.) D.A. Webb cultivars). Similar results were observed in *Pisum sativum*.[37] Copper (35-700 mg kg^{-1}) is highly toxic to pollen germination in tobacco.[38] It is unclear if zucchini exhibits a unique tolerance to copper; importantly, few studies have investigated the potential effects of copper nanomaterials on pollen formation and maturation. Kumbhakar *et al.*

(2016)[39] showed that both copper and cadmium-based NPs reduced pollen fertility in black cumin (*Nigella sativa* L.), both during pollen formation and in developmental maturation process. Similarly, in *Coriandrum sativum* L. CdS NPs and CuO NPs induced physiological alterations and cytological aberrations in meiotic cells, and decreased viability of pollen.[40] The alteration types and frequencies in meiotic cells of *C. sativum* following NPs treatments (0.25-1 mg L^{-1}) were less severe than those reported in *Nigella sativa*.[39] Notably, in the present study the Cu concentration used was specifically selected to be below the limit considered for Cu contamination in soil.[19-20]

Plant biomass and metal content

After flowering, plants were harvested, and the fresh mass of roots and shoots was measured (Table S1-S2). Treatment with CuO, CuO NPs and $CuSO_4$ had no impact on zucchini biomass (fresh weight) compared to untreated control. These results align with much of the present literature, showing that exposure to CuO NPs did not negatively impact the biological parameters in agricultural crops. Tamez et al. (2019)[41] reported no significant changes in zucchini root and leaf biomass upon exposure to comparable concentrations of CuO NPs. Pagano et al. (2016)[21] demonstrated that CuO NPs had no effect on *C. pepo* biomass at a higher concentration (500 mg kg^{-1}) and with an experimental design that provided greater direct interaction between NPs and tissues (vermiculite growth media). Alternatively, studies conducted with the model plant *Arabidopsis thaliana* grown in hydroponic conditions showed a strong reduction in root length after exposure to CuO NPs (10-20 mg L^{-1}).[42] These contrasting results demonstrate the importance of CuO NPs dose to biological response, and also highlight the influence of growth medium, plant species, and the exposure time to observed effects.

The Cu content in different tissues of zucchini plants was determined by Atomic Absorption Spectroscopy (AAS). As shown in Table S3; although there was a trend for increased Cu content of tissues with all Cu treatments, only plant roots from the $CuSO_4$ exposure were significantly increased. To validate the AAS results on flowers, analysis of the Cu content was performed also by Inductively

306 Coupled Plasma Mass Spectrometry (ICP-MS). Here, results show that the Cu content from the CuO
307 NPs and bulk material treatment was 43 and 30% (significant at $p<0.05$) greater than the untreated
308 control, respectively (Table S4). This finding demonstrates that CuO NPs addition to the soil does
309 result in Cu accumulation in the reproductive tissues, although there is no difference based on particle
310 size. However, it should be considered that those results were be impacted by instrument limits of
311 detection and quantitation. A previous study from our group focused on zucchini exposed to
312 nanoscale Cu evaluated a broad set of physiological assays, including chlorophyll content,
313 mitochondrial functionality, and metal content in different plant tissues (roots, stems, leaves), and
314 also demonstrated significant Cu translocation from roots to both stems and leaves.[21]
315
316 *RNA-seq data analysis: critical aspects related to the CuO NP molecular response*

317 Given the evidence of an active translocation of Cu into reproductive tissues, the plant
318 transcriptomic response of different tissues and organs to exposure was evaluated using the high-
319 quality assembly of the *C. pepo* genome (NCBI BioProject PRJNA386743, sequences length 263
320 Mbps; 34240 ORFs) published on Cucurbitgenomics database.[23] Statistical analysis of RNA-seq
321 datasets showed high homogeneity between treatments in the different tissues, with comparable
322 averages and dispersions (Figures S3-S6). After normalization to the untreated control, comparison
323 across CuO NPs, CuO bulk and $CuSO_4$ exposure in roots showed 4420, 6540, and 4747 differentially
324 expressed genes in the three treatments, respectively. In leaves, the CuO NPs treatment showed a
325 lower number of differentially expressed genes compared to the other treatments: 3122 genes were
326 up- or down-regulated with CuO exposure, whereas the values for CuO bulk and $CuSO_4$ were 9924
327 and 9103, respectively. The number of differentially expressed genes in CuO NPs exposed pollen
328 was also markedly lower in comparison to the treatments in the other tissues: 1829, 2112 and 2163
329 respectively for CuO NPs, CuO bulk and $CuSO_4$ treatments. This large quantitative difference in gene
330 expression was certainly related with a larger number of different biological processes performed in

roots and leaves, as compared to pollen, but could be also due to the lower amount of the Cu (in different forms) translocated to pollen.

Venn's diagrams of up- and down-regulated genes in roots (Figure 1) and the relative GO enrichment (Supplementary Information, SI2) data show that the transcripts in common among all the tested conditions were only 4.3% and 16.3% of total genes up- and down-regulated, respectively. In the roots, the specific molecular responses to the three different treatments were largely independent of each other, as shown by the low percentage of gene functions common among all the three conditions tested and by the two-by-two common classes. Metabolic processes and ribosome translation were the most highly represented groups in biological processes related to CuO NPs and CuO bulk (Figure 2; details in Supplementary Information, SI2), together with mitochondrial activity. In the $CuSO_4$ treatment, unlike the NPs and bulk exposure, a nuclear component was represented, and this can be related to greater Cu ion toxicity.[43] The percentage of genes commonly up- or down-regulated in leaves was similar to that observed in roots: 4.7% and 16.4% total shared genes, respectively (Figure 1). The percentage of genes in common between CuO bulk and $CuSO_4$ increased dramatically, both for up- and down-regulated transcripts, to 40.1% and 46.6%, respectively. This observation may correlate with the Cu ion release from the CuO bulk material within the plant tissues, which seems to be higher than for CuO NPs, in spite of the similar dissolution rate in ddH_2O. Genes involved in metabolic and energetic processes are among the more enriched genes; in addition, GO terms related to chloroplast genes are well represented, as are genes for abiotic stimuli response (Figure 2; details in Supplementary Information, SI3). Previous studies with *A. thaliana* highlighted the role of chloroplast as a potential target of ENMs exposure.[44] Wang *et al.* (2016)[45] showed that CuO NPs block electron transport between the two photosystems which can cause an excessive ROS accumulation and oxidative stress, damaging biological molecules and disrupting of cellular metabolism. Furthermore, CuO NPs strongly up-regulate ZAT12, a transcription factor implicated in abiotic stress response, with a key role in ROS signalling pathway and co-expressed with ORF31, a chloroplastic electron carrier involved in photosynthesis that has been identified as a potential

biomarker of ENM exposure.[21] In pollen, the percentage of genes up- or down-regulated common to all treatments increased as compared to the leaves and roots: 25.5% and 33%, respectively (Figure 1). The percentage of genes up- and down-regulated specifically related to CuO NPs response is significant (21.1% and 12.5%), when compared to the other two treatments. This data strengthens the idea that CuO NPs were not only translocated (intact or modified) into the floral parts of the plant, but once there, they trigger a "nanoscale-specific" response which is different from the response observed in roots and leaves. These results likely reflect a multifaceted response, including partial dissolution of CuO NPs and CuO bulk giving rise to a "non-specific Cu response", along with a non-dissolved component exerting a nanoscale-specific response. It is also reasonable to suppose that amount of Cu^{2+} derived from the three treatments increased as a consequence of the interaction with plant organs and tissues.

Pollen has a significantly lower number of expressed genes as compared to the vegetative tissues, but data highlight some pollen-specific functions and other components which have been described as unique to sporophyte tissues.[46] The difference with the leaves was related to the low level of expression of genes involved in energy metabolism, especially photosynthesis, since pollen is not photosynthetically active. The other difference in pollen was the higher expression level of genes with functions in ion transport, cell-wall metabolism, and cytoskeleton dynamics (Figure 2; details in Supplementary Information, SI4). Previous studies showed that polarized internal gradients and/or external fluxes of protons, potassium, and chloride had a role in pollen tube function,[47] but that ion channel and transporter involvement in ion fluxes across the plasma membrane in pollen tubes is still largely unknown. Starch biosynthesis during the final phases of pollen maturation is fundamental because starch is a reserve source of energy for pollen survival and it may also act as a metabolic checkpoint for pollen maturity. This pathway is prematurely aborted whenever starch levels remain below a critical amount, strongly linking pollen viability to starch deficiency.[48] A key aspect of pollen tube tip growth is the constant construction of new cell wall and plasma membrane at the tube apex. Vesicles delivering this material are mediated by the actin cytoskeleton.[49]

383 The whole transcriptome analysis of *C. pepo* treated with CuO NPs showed interesting
384 insights from a functional point of view. Chloroplast and mitochondrial function were critical in
385 regulating the response to CuO NPs and the energy metabolism in all plant tissues, which becomes
386 primarily mitochondrial functionality in pollen formation and development (Figure 2; details in
387 Supplementary Information, SI5). A network analysis produced for chloroplast genes in leaves, and
388 for mitochondrial genes in roots, leaves and pollen, respectively, shows the physical interactions
389 between the reported gene targets (Figures S7-S10). Genes highlighted in heatmaps and Venn's
390 diagrams (Figure 3) showed a certain specificity to CuO NPs response, in particular in roots and
391 leaves. In the case of pollen, the percentage of common regulated genes among CuO NPs, CuO bulk
392 and $CuSO_4$ treatment is increased (Figure 3), suggesting that during translocation from roots to shoots
393 there was an increase in ionic Cu presence. Additional information about potential sensitive targets
394 in pollen development, derived from the study of orthologue genes in the yeast *S. cerevisiae*, were
395 investigated, highlighting a certain level of commonality in the response with the RNA-seq analyses.
396 Results are reported and described in Supplementary information (Table S5, and Figure S11).
397

398 *CuO NPs biotransformation*

399 μ-XRF analyses performed at the TwinMic beamline,[26] an example of which is depicted in
400 Figure 4, showed that in the root sections, Cu in general was mainly detectable on cell walls and more
401 visible in the treatments with $CuSO_4$, followed by nanoparticle and bulk forms where Cu content was
402 very close to TwinMic detection limits; the higher presence of Cu in the treatments with $CuSO_4$ salt
403 is due to the salt dissociation in the soil and followed by ready Cu accumulation in the roots. Notably,
404 the roots were thoroughly washed before the resin embedding procedures to avoid external
405 contamination. Fe was highly present in all root samples, including the controls, likely because it was
406 abundant in the soil. The roots maps for Cu (Figure 4a) are consistent with those obtained by Servin
407 et al (2017).[18] In the flower samples (Figure 4b), it is possible to observe the pollen sacs and the

completely developed pollen grain; one exception is for the $CuSO_4$ treatment, where the pollen sacs were noticeably smaller and possessed fewer pollen grains. Interestingly, Cu was present in the roots, in particular in the cell wall, along with other elements found in literature such as Ca, which is an important cofactor in building of the cell wall.[50] Although the resolution of the maps does not allow nanoparticle visualization, the EXAFS analyses (Table S6, Figure 5) confirm that CuO NPs in the plants were biotransformed. This suggests that cellular and molecular activities remodel and biotransform the nanoparticles. Cu was present in the flowers treated with all the three types of Cu-based materials, but there were minimal differences in the signal intensity and in the localization of the element. The treatment with CuO NPs did not hinder formation of the flower or pollen and did not result in overt phytotoxicity, but there were nanoscale-specific molecular effects at the transcriptomic levels as described by RNA-seq analysis. The same was true for the bulk Cu treatment, although treatment with $CuSO_4$ did appear to negatively affect gamete formation. The idea of a biotransformation of CuO NPs once within the plant tissues has been reported in the literature; Servin et al. (2017) reported that after treatment, transformed CuO NPs products were detected in roots as Cu_2O, Cu_2S and Cu-acetate.[18] These biotransformation processes significantly influence NPs bioavailability and effects in plants, including broad main metabolic and physiological processes, as well as gametogenesis.[18,51]

Figure 5 shows normalized XANES and EXAFS spectra of the plant samples, together with those of the model compounds CuO, CuO NPs and $CuSO_4 \cdot 5H_2O$ and the EXAFS multiparameter fits. Both XANES and EXAFS features show that the CuO NPs structure is closely related to the CuO bulk structure. EXAFS multiparameter fits (Table S6, additional information in Figure S12) were performed on both CuO samples based on the tenorite structure,[52] yielding the same results in terms of interatomic distances and path degeneracies, with both refined parameters closely agreeing with the theoretical ones. EXAFS quantitative results on plant samples (Figure 5, Table S6) clearly indicate that the CuO structure is not fully preserved within the plants tissues, in particular in the roots, and that after uptake, the particles are biotransformed over time, leading to Cu^{2+} release starting in roots

and increasing up to the flower. Specifically, the prominent signal at R > 4.5 Å in the Fourier Transform (FT) spectra in both CuO bulk and NPs is not visible any longer in plant samples. Moreover, the peaks at R< 4.5 Å are markedly weakened. In addition, no overt differences are observable among plant samples treated with two different CuO types. First, shell distances in both roots and flowers are typical of Cu^{2+} in square planar coordination with O and thus compatible with a remnant structure of CuO. However, the Cu local environment in the higher shells shows small differences between roots and flowers. Indeed, a second Cu-O shell path is systematically present in both flowers and roots at significantly different distances: ≈2.7 Å in roots and 2.8 Å in flowers. Moreover, a Cu-Cu path at ≈3.55 Å is always present in roots while the same path could not be fitted in flowers, the only exception being plants treated with $CuSO_4$, where the path distance is much longer (3.79 Å). In shoots of the Cu hyperaccumulator plant *Crassula helmsii*, Kupper at al. (2009)[53] reported Cu^{2+} O ligands at 2.001 Å, indicating Cu bonds with small organic acids. Mijovilovich et al. (2009)[54] studied the leaves of *Noccea caerulescences* (ecotype Ganges), an hyperaccumulator plant of Cd and Zn but sensitive to Cu, reported ligands for Cu^{2+} at 1.9 Å sulfur atoms, indicating ligands with S rich molecules, and at 4.5 Å, a double ligand Cu-Cu that they attributed to Cu biomineralization. These findings do not align with our results and this is likely due to plant species differences; hyperaccumulator plants having a unique and specific metabolic profile that is different from that of non-hyperaccumulator species such as *Cucurbita pepo*.

Environmental implications

Given the essential role of Cu to the plant life cycle and its biotic response to disease, there has been significant interest in its use as a potential nanofertilizer, however, in certain plants and under certain concentrations, phytotoxicity has been observed. In the present study, the effect of three types of Cu (CuO NPs, CuO bulk, and $CuSO_4$) was compared in *C. pepo* using a broad range of physiological and molecular endpoints, with a focus on the process of male gametogenesis and pollen

459 production, which are essential to reproduction and from fruit formation and ultimately, to plant yield.
460 In a dioic species such as zucchini, gamete fertilization depends primarily on pollen quality and
461 vitality of the parental plant, which then mediates fruit production. From the morphological and
462 physiological perspective, as inferred by ESEM and XRF analyses, there were few differences
463 between the three forms of Cu (CuO NPs, CuO bulk and $CuSO_4$) in the roots, but as the Cu was
464 translocated to the flower, the $CuSO_4$ treatment exerted a more marked negative effect on pollen
465 viability. This increasing toxic response likely was a function of the complete dissolution to Cu^{2+} ions
466 in this medium and the increased reactivity of Cu in this form. Conversely, the NP form exerted
467 almost no effects on pollen and exhibited a reduced stimulation of Cu uptake, possibly being a
468 function of Cu complexed to organic ligands within the plant tissues that mitigated chemical
469 dissolution. The CuO bulk material results for the molecular and physiological endpoints were more
470 similar to $CuSO_4$, in spite of the CuO bulk and CuO NPs dissolution behaviour in ddH_2O being quite
471 similar. Interesting, some nanoscale materials release ions at a greater rate than bulk materials, due
472 to increased surface area and volume.[14] However, coatings, complexation and corona formation could
473 modulate dissolution. The transcriptomic analysis of the different tissues and flowers showed that
474 metabolic processes and ribosome translation were highly represented among the most responsive
475 pathways. Chloroplast and especially mitochondrial functions were particularly affected in response
476 to CuO NPs, which agrees with previous data and aligns with the organelles role in energy metabolism
477 in all plant tissues,[45] and specifically in pollen formation and development. In addition, the EXAFS
478 features demonstrate the occurrence of CuO NPs biotransformation, highlighting a similar Cu local
479 environment from roots to flowers. The similarity of the Cu environment after different treatments
480 seemed to depend more on the plant tissue than on the type of treatment, suggesting that the
481 biotransformed Cu environment is reached after substantial dissolution of Cu ions, followed by
482 stabilization of Cu in complexes whose nature is more dependent on the plant characteristics than on
483 the type of treatment. Indeed, the transcriptomic data showed that at the molecular level, the response
484 was partially nanoscale-specific, including in the pollen. Similar phenomena have been reported for

485 other nanomaterials such as CeO_2 NPs and CdS QDs.[25,55] The evidence for the formation of Cu ions
486 when CuO NPs are accumulated by the plants and the fact that still there is a certain level of
487 nanoscale-specific response suggests that *in planta* biotransformation processes are significant and
488 critical to overall plant response. Overall, this suggests nanoscale CuO NPs as nanofertilizers likely
489 presents minimal concerns to general plant health. A thorough and mechanistic understanding of these
490 processes such as that provided by this study will be necessary to ensure the safe and sustainable
491 application of Cu-based and other nanoscale materials in nano-enabled agricultural strategies.
492
493
494 **Acknowledgements**
495 LP acknowledges the support of FIL ("Fondi Locali per la Ricerca") 2018. MM acknowledges
496 ELETTRA Sincrotrone Trieste beamlines TwinMic (proposal 20195157) and XRF (proposal
497 20195260) for CuO experiments on zucchini plants. GOL and MM acknowledge for XAS
498 experiments on bulk samples were performed on LISA CRG beamline at the European Synchrotron
499 Radiation Facility (ESRF), Grenoble, France during experiment EV-366. JCW acknowledges USDA
500 Hatch CONH00147. The present study has benefited from the equipment and framework of the
501 COMP-HUB Initiative, funded by the 'Departments of Excellence' program of the Italian Ministry
502 for Education, University and Research (MIUR, 2018-2022).
503
504 **Authors contribution**
505 MM, LP, NM and JCW coordinated the study and designed the experiments. RR, LP and RD
506 performed individual experiments and analysed the physiological and molecular data in with
507 collaboration of MM and RRu. AG, GA, performed the synchrotron analyses in Trieste with
508 collaboration of SP, GG and VB. AP, FA and GOL (remotely) performed the XAS measurements at
509 LISA BM08 beamline at ESRF; GOL performed EXAFS data analysis in collaboration with FA. All
510 authors contributed to manuscript revision and approved the final version.

511

512 **Conflict of interest**

513 The authors declare no conflict of interest.

514

515

516 **Supplementary Information (SI) description:**

517 *Supplementary information included* (SI1):

518 Method section and results for qPCR of genes involved in gametogenesis

519 Results of LCF analysis of XANES spectra

520 Figure S1: CuO nanoparticles visualization by TEM

521 Figure S2: ESEM micrographs pollen grains and pollen viability assay

522 Figure S3: Statistics of the genes datasets from roots samples

523 Figure S4: Statistics of the genes datasets from leaves samples

524 Figure S5: Statistics of the genes datasets from pollen samples

525 Figure S6: PCA of all data profiles

526 Figure S7: Gene network of chloroplast targets observed in leaves treated with CuO NPs

527 Figure S8: Gene network of mitochondrial targets observed in roots treated with CuO NPs

528 Figure S9: Gene network of mitochondrial targets observed in leaves treated with CuO NPs

529 Figure S10: Gene network of mitochondrial targets observed in pollen treated with CuO NPs

530 Figure S11: Heatmap transciprotmics genes involved in meiosis and gametogenesis

531 Figure S12: XANES fits and relative K-edge data

532 Table S1: Biomass of roots and shoots

533 Table S2: Flower biomass

534 Table S3: Copper concentration measured in roots, shoots and flowers by AAS

535 Table S4: Copper concentration measured in flowers by ICP-MS

536 Table S5: Genes' information and primer sequences utilized in Real time PCR assay

Table S6: EXAFS multiparameter fit details for studied samples and reference compounds

Supplementary information reported in excel format:

Supplementary Information 2 (SI2): GO analysis of up- and down-regulated genes exposed to CuO NPs, CuO bulk and $CuSO_4$ in roots.

Supplementary Information 3 (SI3): GO analysis of up- and down-regulated genes exposed to CuO NPs, CuO bulk and $CuSO_4$ in leaves.

Supplementary Information 4 (SI4): GO analysis of up- and down-regulated genes exposed to CuO NPs, CuO bulk and $CuSO_4$ in pollen.

Supplementary Information 5 (SI5): *A. thaliana* ortholog genes analysis of relevant chloroplast and mitochondrial targets isolated from *C. pepo* exposed to CuO NPs, CuO bulk and $CuSO_4$ in roots, leaves and pollen.

References

1. Lowry, G. V., Avellan, A., Gilbertson, L. M. Opportunities and challenges for nanotechnology in the agri-tech revolution. *Nat. Nanotechnol*., **2019**, 14, 17–522.
2. Adisa, I.; Pullagurala, V.L.R.; Peralta-Videa, J.R.; Dimkpa, C.O.; Ma, C.; Elmer, W.H.; Gardea-Torresdey J.L.; White, J.C. **2019**. Recent advances in nano-enabled fertilizers and pesticides: A critical review of mechanisms of action. *Environ. Sci.: Nano*. 6, 2002.
3. Dimkpa, C.O., Bindraban, P.S. Nanofertilizers: New Products for the Industry? *J Agric Food Chem*. **2018**, 66(26), 6462-6473. doi: 10.1021/acs.jafc.7b02150.

4. Rui, M.; Ma, C.; White, J.C.; Tang, X.; Yang, J.; Jiang, F.; Hao, Y.; Ali, A.; Rui, Y.; Cao, W.; Xing, B. Metal oxide nanoparticles alter peanut (Arachis hypogaea L.) physiological response and reduce nutritional quality: A life cycle study. *Environ. Sci.: Nano*. **2018**, 5, 2088-2102.
5. Keller, A.A.; McFerran, S.; Lazareva, A.; Suh, S. Global life cycle releases of engineered nanomaterials. *J. Nanopart. Res.*, **2013**, 15, 1692−1709.
6. Gardea-Torresdey, J.L.; Rico, C.M.; White, J.C. Trophic transfer, transformation, and impact of engineered nanomaterials in terrestrial environments. *Environ. Sci. Technol*., **2014**, 48, 2526–2540.
7. Hawthorne, J.; De la Torre Roche, R.; Xing, B.; Newman, L.A.; Ma, X.; Majumdar, S.; Gardea-Torresdey, J.; White, J.C. Particle-size dependent accumulation and trophic transfer of cerium oxide through a terrestrial food chain. *Environ. Sci. Technol*. **2014**, 48, 13102-13109.
8. Ma, C.; White, J.C.; Zhao, J.; Zhao, Q.; Xing, B. Uptake of Engineered Nanoparticles by Food Crops: Characterization, Mechanisms, and Implications. *Annu. Rev. Food Sci. Technol*. **2018**, 9, 129–53.
9. Majumdar, S.; Ma, C.; Villani, M.; Zuverza-Mena, N.; Pagano, L.; Huang, Y.; Zappettini, A.; Keller, A.A.; Marmiroli, N.; Dhankher, O.P.; White, J.C. Surface coating determines the response of soybean plants to cadmium sulfide quantum dots. *NanoImpact*, **2019**, 14, 100151. Doi: 10.1016/j.impact.2019.100151.
10. Servin, A. D.; White, J. C. Nanotechnology in agriculture: Next steps for understanding engineered nanoparticle exposure and risk. *NanoImpact*. **2016**, 1, 9−12.
11. Elmer, W.; De la Torre-Roche, R.; Pagano, L.; Majumdar, S.; Zuverza-Mena, N.; Dimkpa, C.; Gardea-Torresdey, J.; White, J. C. Effect of metalloid and metallic oxide nanoparticles on Fusarium wilt of watermelon. *Plant Dis.* **2018**, 102 (7), 1394−1401.
12. Kah, M.; Tufenkji, N.; White, J.C. Nano-enabled strategies to enhance crop nutrition and protection. *Nat. Nanotechnol*., **2019**, 14, 532–540.

13. Ma, C.; Borgatta, J.; Hudson, B.G.; Abbaspour-Tamijani, A.; De La Torre-Roche, R; Zuverza-Mena N.; Shen, Y.; Elmer, W.; Xing, B.; Mason, S.E.; Hamers, R.J. White J.C. Advanced material modulation of nutritional and phytohormone status alleviates damage from soybean sudden death syndrome. *Nat. Nanotechnol*. **2020**. Doi: 10.1038/s41565-020-00776-1.

14. Borgatta, J.; Ma, C.; Hudson-Smith, N.; Elmer, W.; Plaza Perez, C.D.; De La Torre-Roche, R.; Zuverza-Mena, N.; Haynes, C.L.; White, J.C.; Hamers, R.J. Copper Based Nanomaterials Suppress Root Fungal Disease in Watermelon (Citrullus lanatus): Role of Particle Morphology, Composition and Dissolution Behavior. *ACS Sus Chem Eng* **2018,** 6 (11), 14847-14856. Doi: 10.1021/acssuschemeng.8b03379

15. Ma, C.; Borgatta, J.; De La Torre-Roche, R.; Zuverza-Mena, N.; White, J.C.; Hamers, R.J; Elmer, W. Time-Dependent Transcriptional Response of Tomato (Solanum lycopersicum L.) to Cu Nanoparticle Exposure upon Infection with Fusarium oxysporum f. sp. Lycopersici. *ACS Sus Chem Eng* **2019,** 7 (11), 10064-10074. Doi: 10.1021/acssuschemeng.9b01433.

16. Huang Y.; Zhao, L.; Keller, A.A. Interactions, Transformations, and Bioavailability of Nano-Copper Exposed to Root Exudates. *Environ Sci Technol*., **2017** 51 (17), 9774-9783. Doi: 10.1021/acs.est.7b02523.

17. Huang, Y.; Li, W.; Minakova, A.S.; Anumol, T.; Keller, A.A. Quantitative analysis of changes in amino acids levels for cucumber (*Cucumis sativus*) exposed to nano copper. *NanoImpact*, **2018**, 12, 9-17. doi: 10.1016/j.impact.2018.08.008.

18. Servin, A.D.; Pagano, L.; Castillo-Michel, H.; De la Torre-Roche, R.; Hawthorne, J.; Hernandez-Viezcas, J.A.; Loredo-Portales, R.; Majumdar, S.; Gardea-Torresdey, J.L.; Dhankher, O.P.; White, J.C. Weathering in soil increases nanoparticle CuO bioaccumulation within a terrestrial food chain. *Nanotoxicology*, **2017**, 11, 98–111. Doi: 10.1080/17435390.2016.1277274.

19. McLean, E.J.; Bledsoe, B.E. Behavior of Metals in Soils. *United States Environmental Protection Agency*, **1992**, EPA/540/S-92/018.

20. Shabbir, Z.; Sardar, A.; Shabbir, A.; Abbas, G.; Shamshad, S.; Khalid, S.; Natasha; Murtaza, G.; Dumat, C.; Shahid, M. Copper uptake, essentiality, toxicity, detoxification and risk assessment in soil-plant environment. *Chemosphere*, **2020**, 259, 127436.

21. Pagano, L.; Servin, A. D.; De La Torre-Roche, R.; Mukherjee, A.; Majumdar, S.; Hawthorne, J.; Marmiroli, M.; Maestri, E.; Marra, R. E.; Isch, S. M.; Dhankher, O. P.; White, J. C.; Marmiroli, N. Molecular Response of Crop Plants to Engineered Nanomaterials. *Environ. Sci. Technol.* **2016**, *50* (13), 7198–7207. Doi: 10.1021/acs.est.6b01816.

22. Peterson, R.; Slovin, J. P.; Chen, C. A Simplified Method for Differential Staining of Aborted and Non-Aborted Pollen Grains. *Int. J. Plant Biol.* **2010**, 1 (2), 66–69. Doi: 10.4081/pb.2010.e13.

23. Montero-Pau, J.; Blanca, J.; Bombarely, A.; Ziarsolo, P.; Esteras, C.; Martí-Gómez, C.; Ferriol, M.; Gómez, P.; Jamilena, M.; Mueller, L.; Picó, B.; Cañizares, J. De Novo Assembly of the Zucchini Genome Reveals a Whole-Genome Duplication Associated with the Origin of the Cucurbita Genus. *Plant Biotechnol. J.* **2018**, *16* (6), 1161–1171. Doi: 10.1111/pbi.12860.

24. Kurth, T.; Weiche, S.; Vorkel, D.; Kretschmar, S.; Menge, A. Histology of plastic embedded amphibian embryos and larvae. *Genesis*. **2012**, 50, 235-250. doi:10.1002/dvg.20821.

25. Marmiroli, M.; Lepore, G.O.; Pagano, L.; d'Acapito, F.; Gianoncelli, A.; Villani, M.; Lazzarini, L.; White, J.C.; Marmiroli, N. The fate of CdS Quantum Dots in plants as revealed by Extended X-ray Absorption Fine Structure (EXAFS) analysis. *Environ. Sci.: Nano*, **2020**. Doi: 10.1039/C9EN01433K.

26. Gianoncelli, A., Kourousias, G., Merolle, L., Altissimo, M. & Bianco, A. Current status of the TwinMic beamline at Elettra: a soft X-ray transmission and emission microscopy station. *J. Synchrotron Rad*. **2016**, 23, 1526-1537. doi: 10.1107/S1600577516014405.

637 27. Gianoncelli, A.; Castaing, J.; Bouquillon, A.; Polvorinos, A.; Walter, P. Quantitative
638 elemental analysis of Della Robbia glazes with a portable XRF spectrometer and its
639 comparison to PIXE methods. *X-Ray Spectrom*., **2006**. 35: 365-369. doi:10.1002/xrs.920.
640 28. Solé, V.; Papillon, E.; Cotte, M.; Walter, P.; Susini, J. A Multiplatform Code for the Analysis
641 of Energy-Dispersive X-ray Fluorescence Spectra. *Spectrochimica Acta Part B: Atomic*
642 *Spectroscopy*. **2007**. 62. 63-68. Doi: 10.1016/j.sab.2006.12.002.
643 29. Karydas, A.; Czyzycki, M.; Leani, J.; Migliori, A.; Osan, J.; Bogovac, M.; Wrobel, P.; Vakula,
644 N.; Padilla A.R.; Menk, R.H.; Gol, M.; Antonelli, M.; Tiwari, M.; Caliri, C.; Vogel-Mikus,
645 K.; Darby, I. An IAEA multi-technique X-ray spectrometry endstation at Elettra Sincrotrone
646 Trieste: benchmarking results and interdisciplinary applications. *J. Synchrotron Radiation*.
647 **2017**. 25. 189. 10.1107/S1600577517016332.
648 30. Ravel, B.; Newville, M. ATHENA and ARTEMIS: Interactive graphical data analysis using
649 IFEFFIT. *Phys. Scr*. **2006**, 115, 1007-1010. Doi: 10.1238/Physica.Topical.115a01007.
650 31. d'Acapito, F., Lepore, G.O., Puri, A., Laloni, A., La Mannna, F., Dettona, E., De Luisa, A.,
651 Martin, A. The LISA beamline at ESRF. *J. Synchrotron Radiat.* **2019**, 26, 551-558.
652 32. Puri, A.; Lepore, G. O.; d'Acapito, F. The New Beamline LISA at ESRF: Performances and
653 Perspectives for Earth and Environmental Sciences. *Condens Matter* **2019**, 4, 12-19.
654 33. Lee, P. A.; Citrin, P. H.; Eisenberger, P. T.; Kincaid, B. M. Extended x-ray absorption fine
655 structure - its strengths and limitations as a structural tool. *Revi Mod Phys* **1981**, 53, 769-806.
656 34. Ravel, B. ATOMS: crystallography for the X-ray absorption spectroscopist. J Synchr Rad
657 **2001** 8, 314–316.
658 35. Ankudinov, A.L.; Ravel, B.; Rehr, J.J.; Conradson, S.D. Real-space multiple-scattering
659 calculation and interpretation of x-ray-absorption near-edge structure. *Phys Rev B* **1998**, 58,
660 7565-7576.
661 36. Sharafi, Y. Effects of Copper and Leadon Pollen Germination Traits in Almond Cultivars. *J.*
662 *Nuts Relat. Sci.* **2014**, *5* (2), 67–73.

663 37. Sabrine, H.; Afif, H.; Mohamed, B.; Hamadi, B.; Maria, H. Effects of Cadmium and Copper
664 on Pollen Germination and Fruit Set in Pea (Pisum Sativum L.). *Sci. Hortic.* **2010**, *125* (4),
665 551–555. doi: 10.1016/j.scienta.2010.05.031.
666 38. Breygina, M.; Matveyeva, N.; Polevova, S.; Meychik, N.; Nikolaeva, Y.; Mamaeva, A.;
667 Yermakov, I. Ni^{2+} Effects on Nicotiana Tabacum L. Pollen Germination and Pollen Tube
668 Growth. *BioMetals* **2012**, *25* (6), 1221–1233. Doi: 10.1007/s10534-012-9584-0.
669 39. Kumbhakar, D. V.; Datta, A. K.; Mandal, A.; Das, D.; Gupta, S.; Ghosh, B.; Halder, S.; Dey,
670 S. Effectivity of Copper and Cadmium Sulphide Nanoparticles in Mitotic and Meiotic Cells
671 of Nigella Sativa L. (Black Cumin) – Can Nanoparticles Act as Mutagenic Agents? *J. Exp.*
672 *Nanosci.* **2016**, *11* (11), 823–839. Doi: 10.1080/17458080.2016.1149236.
673 40. Pramanik, A.; Datta, A. K.; Das, D.; Kumbhakar, D. V.; Ghosh, B.; Mandal, A.; Gupta, S.;
674 Saha, A.; Sengupta, S. Assessment of Nanotoxicity (Cadmium Sulphide and Copper Oxide)
675 Using Cytogenetical Parameters in Coriandrum Sativum L. (Apiaceae). *Cytol. Genet.* **2018**,
676 *52* (4), 299–308. Doi: 10.3103/S0095452718040084.
677 41. Tamez C, Hernandez-Molina M, Hernandez-Viezcas J.A, Gardea-Torresday J.L. Uptake,
678 transport, and effects of nano-copper exposure in zucchini (Cucurbita pepo). *Sci Total*
679 *Environ*. **2019**, 665, 100-106. Doi: 10.1016/j.scitotenv.2019.02.029
680 42. Tang, Y.; He, R.; Zhao, J.; Nie, G.; Xu, L.; Xing, B. Oxidative Stress-Induced Toxicity of
681 CuO Nanoparticles and Related Toxicogenomic Responses in Arabidopsis Thaliana. *Environ.*
682 *Pollut.* **2016**, *212*, 605–614. Doi: 10.1016/j.envpol.2016.03.019.
683 43. Dutta, S.; Mitra, M.; Agarwal, P.; Mahapatra, K.; De, S.; Sett, U.; Roy, S. Oxidative and
684 Genotoxic Damages in Plants in Response to Heavy Metal Stress and Maintenance of Genome
685 Stability. *Plant Signal. Behav.* **2018**, *13* (8), 1–17. Doi: 10.1080/15592324.2018.1460048.
686 44. Ruotolo, R.; Maestri, E.; Pagano, L.; Marmiroli, M.; White, J. C.; Marmiroli, N. Plant
687 Response to Metal-Containing Engineered Nanomaterials: An Omics-Based Perspective.
688 *Environ. Sci. Technol.* **2018**, *52* (5), 2451–2467. Doi: 10.1021/acs.est.7b04121.

689 45. Wang, Z.; Xu, L.; Zhao, J.; Wang, X.; White, J. C.; Xing, B. CuO Nanoparticle Interaction
690 with Arabidopsis Thaliana: Toxicity, Parent-Progeny Transfer, and Gene Expression.
691 *Environ. Sci. Technol.* **2016**, *50* (11), 6008–6016. Doi: 10.1021/acs.est.6b01017.
692 46. Honys, D.; Twell, D. Comparative Analysis of the Arabidopsis Pollen Transcriptome. *Plant*
693 *Physiol.* **2003**, *132* (June), 640–652. Doi: 10.1104/pp.103.020925.
694 47. Hepler, PK; Vidali, L; Cheung, AY. Polarized cell growth in higher plants. *Annual Rev. Cell.*
695 *Dev. Biol. **2001,*** 17: 159–187
696 48. Wen, L. Y.; Chase, C. D. Mitochondrial Gene Expression in Developing Male Gametophytes
697 of Male-Fertile and S Male-Sterile Maize. *Sex. Plant Reprod.* **1999**, *11* (6), 323–330. Doi:
698 10.1007/s004970050159.
699 49. Da Costa-Nunes, J. A.; Grossniklaus, U. Unveiling the Gene-Expression Profile of Pollen.
700 *Genome Biol.* **2003**, *5* (1), 9–11. Doi: 10.1186/gb-2003-5-1-205.
701 50. Hepler P.K. Calcium: A Central Regulator of Plant Growth and Development. *The Plant Cell*.
702 **2005**, 17(8) 2142-2155. Doi: 10.1105/tpc.105.032508.
703 51. Dai, Y.; Zhao, J.; Liu, X.; Yu, X.; Jiang, Z.; Bu, Y.; Xu, Z.; Wang, Z.; Zhu, X.; Xing, B.
704 Transformation and Species Identification of CuO Nanoparticles in Plant Cells (Nicotiana
705 Tabacum). *Environ. Sci. Nano* **2019**, *6* (9), 2724–2735. Doi: 10.1039/c9en00781d.
706 52. Wyckoff, R. W. G. Crystal Structures 1963. 1, 85–237. Second edition. Interscience
707 Publishers, New York.
708 53. Küpper, H.; Götz, B.; Mijovilovich, A.; Küpper, F.C.; Meyer-Klaucke, W. Complexation and
709 Toxicity of Copper in Higher Plants. I. Characterization of Copper Accumulation, Speciation,
710 and Toxicity in *Crassula helmsii* as a New Copper Accumulator. *Plant. Physiol.* **2009**, 151
711 (2) 702-714. Doi: 10.1104/pp.109.139717.
712 54. Mijovilovich, A.; Leitenmaier, B.; Meyer-Klaucke, W.; Kroneck, P.M.H.; Götz, B.; Küpper,
713 H. Complexation and Toxicity of Copper in Higher Plants. II. Different Mechanisms for
714 Copper versus Cadmium Detoxification in the Copper-Sensitive Cadmium/Zinc

715 Hyperaccumulator *Thlaspi caerulescens* (Ganges Ecotype). *Plant. Physiol.* **2009,** 151 (2),
716 715–731. Doi/10.1104/pp.109.144675.
717 55. Servin, A.D.; De la Torre-Roche, R.; Castillo-Michel, H.; Pagano, L.; Hawthorne, J.;
718 Musante, C.; Pignatello, J.; Uchimiya, M.; White, J.C. Exposure of agricultural crops to
719 nanoparticle CeO_2 in biochar-amended soil. *Plant Physiol. Biochem*., **2017**, 110, 147-157.
720 Doi: 10.1016/j.plaphy.2016.06.003.
721

722

723 **Figure captions:**

724 Figure 1. Comparison of high-throughput transcriptional datasets related to the molecular response
725 of *C. pepo* in condition of treatment with CuO NPs, CuO bulk and $CuSO_4$, in the roots (a), leaves (b),
726 pollen (c), represented with Venn's diagrams. Up-regulated and down-regulated genes are reported
727 on left and right side, respectively. Percentage of identity between CuO NPs, CuO bulk and $CuSO_4$
728 is also reported. Data were normalized on the untreated controls, with a 2.3 threshold of raw data (in
729 log2). Data highlighted an increase in the percentage of common genes involved in the response to
730 the three different Cu-based forms from roots to pollen, suggesting an increased bioavailability of
731 free Cu in the plant shoots.

732

733 Figure 2. GO biological processes expressed in percentage (%) of gene cluster enriched, related to
734 roots (a), leaves (b), and pollen (c) related to the treatment with 100 mg kg^{-1} of CuO NPs. Up-
735 regulated and down-regulated genes are reported as blue and orange bars, respectively. Additional
736 details related to GO analyses in the different tissues are available in Supplementary Information,
737 SI2-SI4.

738

739 Figure 3. Heatmaps and Venn's diagrams comparison of the genes involved in chloroplast functions
740 in response to CuO NPs, CuO bulk and $CuSO_4$, in leaves (a), and in mitochondrial functions identified
741 in roots (b), leaves (c) and pollen (d) tissues. Data related to the specific genes are reported in
742 Supplementary Information, SI5. Data confirmed the increase in percentage of common modulated
743 genes from roots to pollen in response to the three different Cu-based forms utilized for the treatments.

744

745 Figure 4. μ-XRF maps of (a) roots and (b) flowers from plants treated with CuO NPs. Names of the
746 mapped elements are on top of each figure. The maps are related to the black and white square on top
747 left (Abs) which is the 20x image of the cells in the root tissue and pollen sac tissues treated with
748 CuO NPs. Cu map is always the last in the second row for (a) and (b).

749

750 Figure 5. XANES spectra of the measured samples and model compounds (a). Cu K-edge k^2-weighted
751 EXAFS region (b) and Fourier transforms (c) of plant tissues and model compounds. Solid lines are
752 data, red lines are fits. Energy was calibrated with a Cu reference foil (8978.9 eV). In order to
753 minimize beam-induced damage, spectra of samples were acquired at 80 K with a constant k step of
754 0.05 $Å^{-1}$ up to a maximum k value of 12.5 $Å^{-1}$ for plant tissues while model compounds were measured
755 at room temperature with a k step of 0.03 $Å^{-1}$ up to k=18 $Å^{-1}$. Plant samples were measured in the
756 fluorescence mode with a 12-element HP-Ge detector.

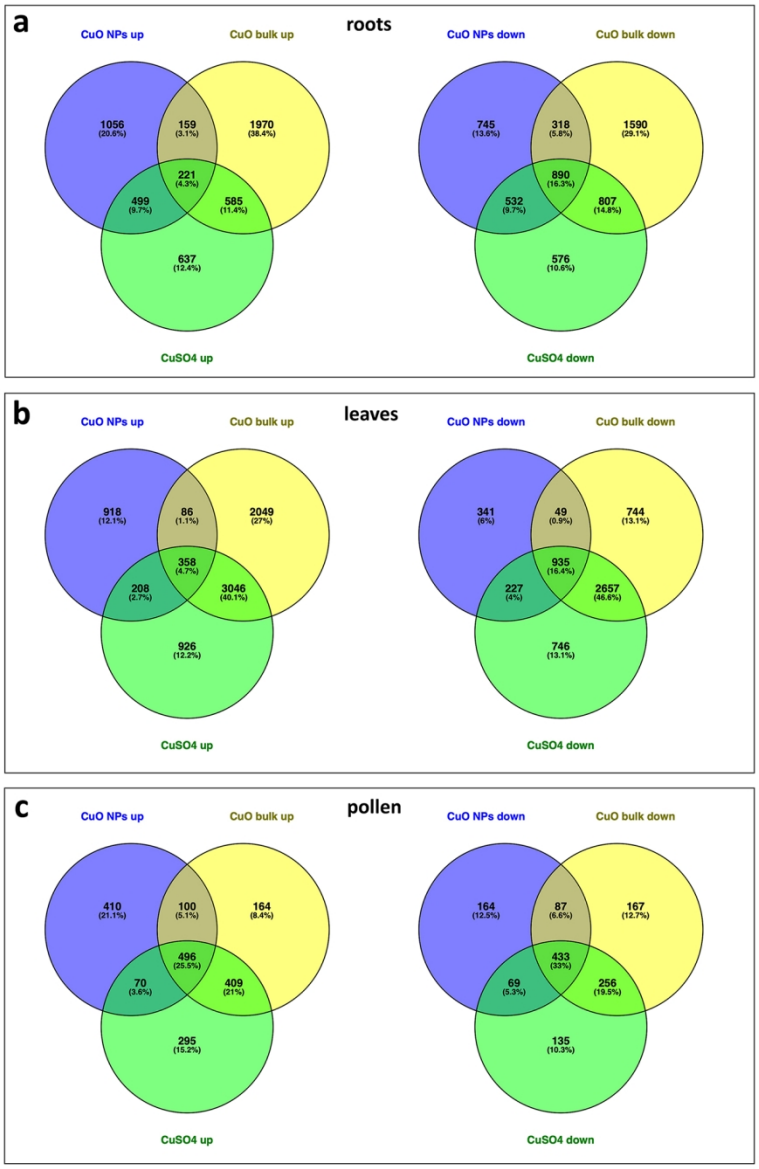

Figure 1. Comparison of high-throughput transcriptional datasets related to the molecular response of C. pepo in condition of treatment with CuO NPs, CuO bulk and CuSO4, in the roots (a), leaves (b), pollen (c), represented with Venn's diagrams. Up-regulated and down-regulated genes are reported on left and right side, respectively. Percentage of identity between CuO NPs, CuO bulk and CuSO4 is also reported. Data were normalized on the untreated controls, with a 2.3 threshold of raw data (in log2). Data highlighted an increase in the percentage of common genes involved in the response to the three different Cu-based forms from roots to pollen, suggesting an increased bioavailability of free Cu in the plant shoots.

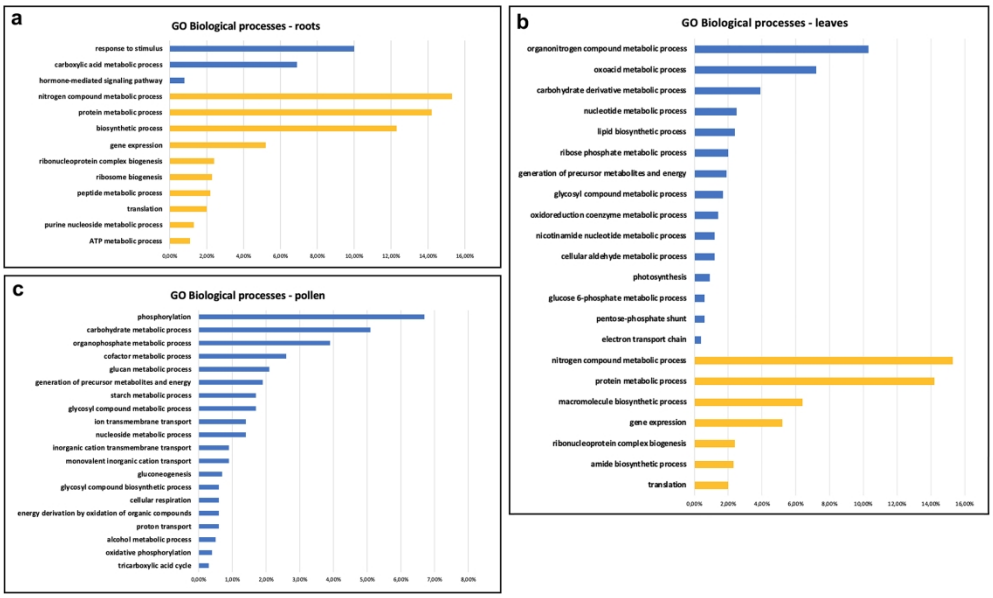

Figure 2. GO biological processes expressed in percentage (%) of gene cluster enriched, related to roots (a), leaves (b), and pollen (c) related to the treatment with 100 mg kg-1 of CuO NPs. Up-regulated and down-regulated genes are reported as blue and orange bars, respectively. Additional details related to GO analyses in the different tissues are available in Supplementary Information, SI2-SI4.

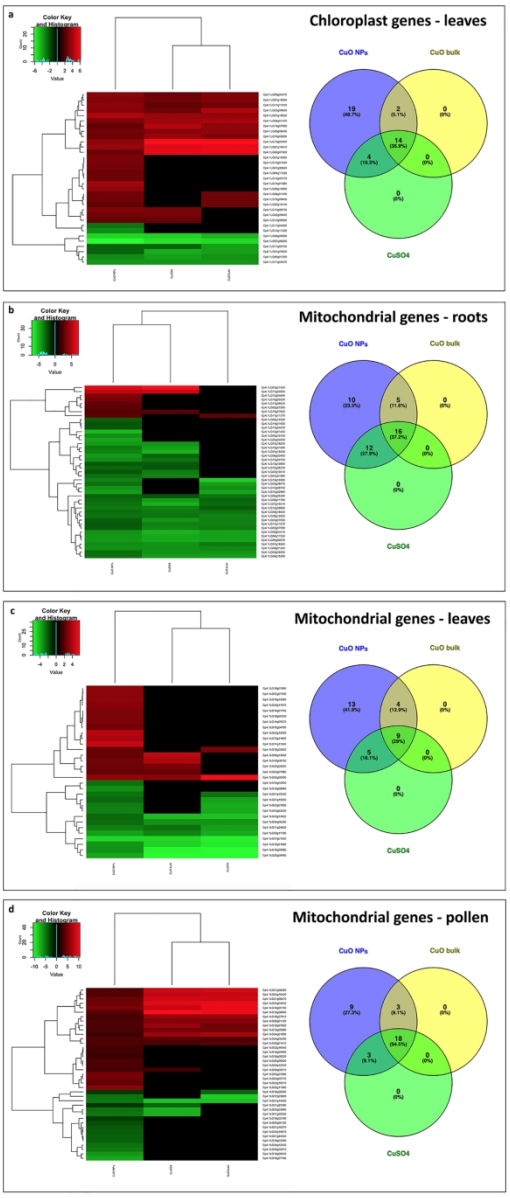

Figure 3. Heatmaps and Venn's diagrams comparison of the genes involved in chloroplast functions in response to CuO NPs, CuO bulk and CuSO4, in leaves (a), and in mitochondrial functions identified in roots (b), leaves (c) and pollen (d) tissues. Data related to the specific genes are reported in Supplementary Information, SI5. Data confirmed the increase in percentage of common modulated genes from roots to pollen in response to the three different Cu-based forms utilized for the treatments.

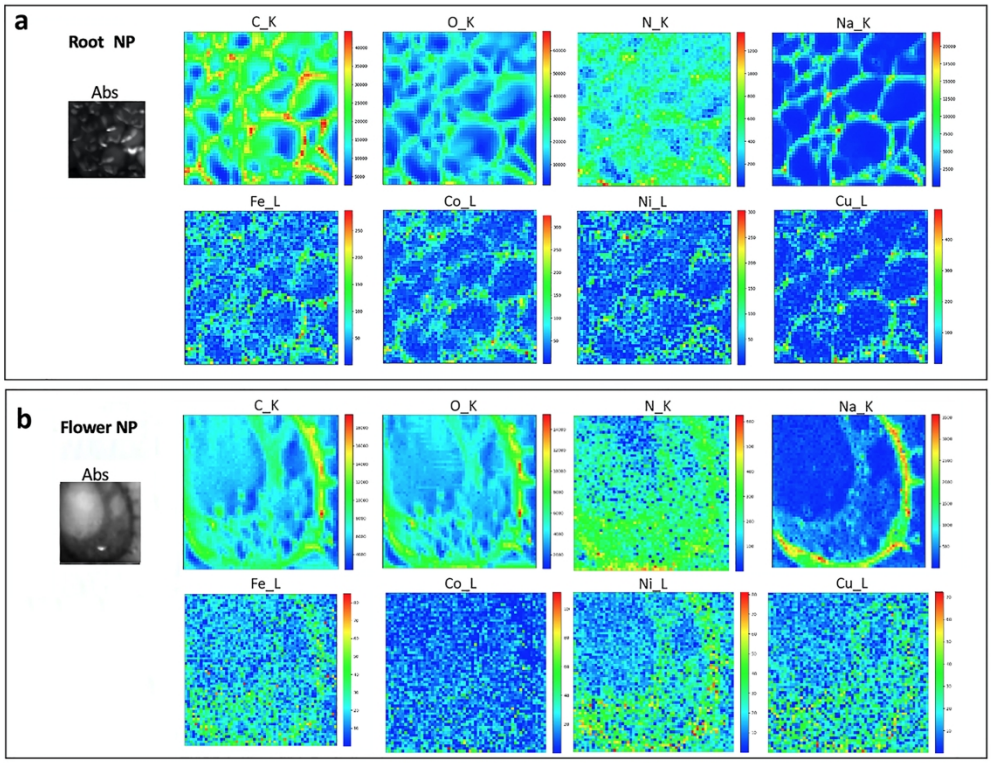

Figure 4. μ-XRF maps of (a) roots and (b) flowers from plants treated with CuO NPs. Names of the mapped elements are on top of each figure. The maps are related to the black and white square on top left (Abs) which is the 20x image of the cells in the root tissue and pollen sac tissues treated with CuO NPs. Cu map is always the last in the second row for (a) and (b).

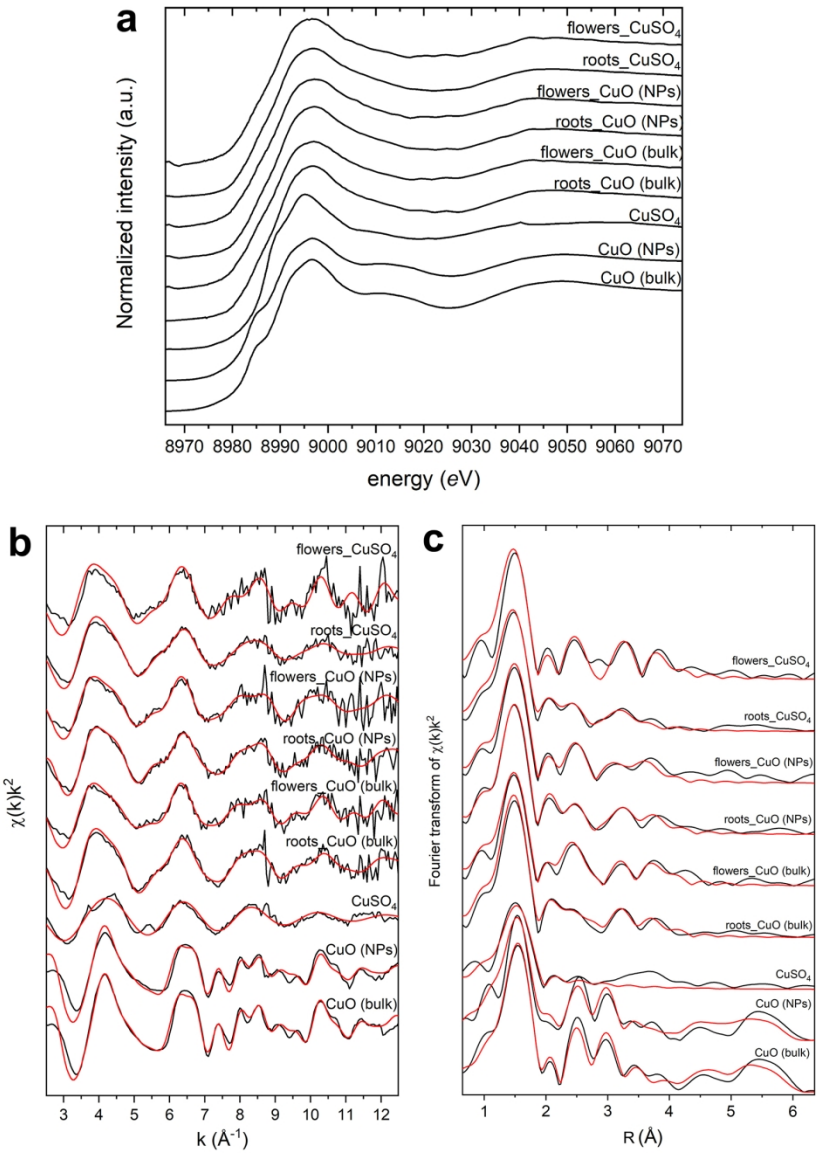

Figure 5. XANES spectra of the measured samples and model compounds (a). Cu K-edge k2-weighted EXAFS region (b) and Fourier transforms (c) of plant tissues and model compounds. Solid lines are data, red lines are fits. Energy was calibrated with a Cu reference foil (8978.9 eV). In order to minimize beam-induced damage, spectra of samples were acquired at 80 K with a constant k step of 0.05 Å-1 up to a maximum k value of 12.5 Å-1 for plant tissues while model compounds were measured at room temperature with a k step of 0.03 Å-1 up to k=18 Å-1. Plant samples were measured in the fluorescence mode with a 12-element HP-Ge detector.